Resonant Frequency Modulation in Inductive Vibration Power Generator via Resistive Impedance Control

Takeaki Yajima, *Member, IEEE*

***Abstract*—Resonant frequency modulation is indispensable for vibration power generators using inductive coils to maintain maximum power extraction against environmental fluctuation. We have shown that by inserting a fixed reactance element in series with an inductive vibration power generator, its resonant frequency can be modulated only by controlling the resistive impedance of the power extraction circuit. The upper limit of the frequency modulation only by resistive impedance was analytically shown and verified by simulation and experiments. For the purpose of comparison between different devices, the figures of merit for electrical frequency modulation capability were also proposed, which are applicable both to resistive impedance control and to complex impedance control. The figure of merit can predict whether the specific harvester device is suitable for electrical frequency modulation or requires mechanical modulation, and the prediction was verified by experiments with two types of harvester devices. The resonant frequency modulation only by changing resistive impedance is more practical than the previously reported methods via complex impedance variation, and readily implemented by power extraction circuits with simple switching operation.**

***Index Terms*—Electrical modulation, electromagnetic induction, energy harvesting, impedance matching, maximum power tracking, power extraction circuit, resonant frequency modulation, vibration power.**

I. Introduction

ENERGY harvesting is attracting attention as a clean energy source for edge devices. In particular, vibration power generation [1], which generates electricity from vibration and mechanical motion, is gaining importance as a complementary technology to the preceding photoelectric and thermoelectric power generation. There are two types of vibration power generation: inductive, which generates induced electromotive force from changes in magnetic flux [2], [3], and capacitive, which uses the piezoelectric effect [4], [5] or electrostatic induction [6], [7], [8]. Inductive vibration power generation has a simple structure consisting of a spring and a magnet and is regarded as a practical device for vibration energy harvesting.

In inductive vibration power generation, mechanical resonance maximizes the vibration displacement, allowing even a small-size generating element to generate a large amount of power. Under the constant amplitude of vibration acceleration, the vibration displacement becomes smaller in a square of the frequency. Therefore, to obtain the maximum amount of power generation from a given vibration space, it is necessary to increase the Q value and increase the vibration amplitude at higher frequencies. However, as the Q value is increased, the frequency band of resonance becomes narrower, and even a small deviation from the ambient vibration frequency can cause fatal problems. To solve this problem, modulation technology of the resonance frequency is important.

Mechanical modulation is often used to modulate the mechanical resonance frequency in inductive vibration power generation [9]. However, such a mechanical method is often incompatible with the miniaturization of power generation elements. Therefore, a technique to electrically modulate the mechanical resonance frequency has been proposed, and theoretical construction and empirical experiments have been conducted [10], [11], [12], [13], [14], [15]. The essence of this technique is to maintain resonance for arbitrary changes in ambient frequency via impedance matching between the vibrating element and the power extraction circuit. Impedance matching can actually be achieved by inserting a capacitance C or inductance L in series with the load R, thereby modulating the resonance frequency. In reality, the winding resistance of the coil and the electromechanical coupling constant limit the modulation range of the resonant frequency [10], [14].

Thus, the studies on resonant frequency modulation have been conducted mainly by *LCR* tuning. However, for small-sized generators, it is appropriate to use fixed values for L and C or coarse discrete control due to their large size. The fine modulation of resonance frequency should rather be performed by R-tuning because it can be easily realized by relatively simple control of switching circuits, such as a magnetic flux extraction circuit that extracts the energy accumulated in the inductor of the generator element [16], [17]. Indeed, the effective R value of these switching circuits can be varied via switching frequency because the

Manuscript received 25 July 2023; revised 4 September 2023; accepted 3 October 2023. Date of publication 9 October 2023; date of current version 6 December 2023. This work was supported in part by Japan Science and Technology Agency under Grant JPMJCR21Q2, in part by Regional Innovation Ecosystem Formation Program in Kanazawa University, Japan, and in part by New Energy and Industrial Technology Development Organization under Grant JPNP22100841-0. Recommended for publication by Associate Editor K.-H. Chen.

The author is with the Department of Electrical and Electronic Engineering, Kyushu University, Fukuoka 819-0395, Japan (e-mail: yajima@ed.kyushu-u.ac.jp).

Color versions of one or more figures in this article are available at https://doi.org/10.1109/TPEL.2023.3322704.

Digital Object Identifier 10.1109/TPEL.2023.3322704

switching frequency determines the average extraction current from the inductor under discontinuous current mode. For example, if we denote the switching period by t_0 and the inductive voltage by $V(t)$, which evolves in a time scale longer than t_0, the average current through the inductor is approximately given by $V(t)t_0/(2L)$ as long as $t_0 < L/R_L$. Then, the effective R value of this switching circuit is given by $(2L)/t_0$, which can be controlled via t_0. It should be noted that the resonance frequency modulation via R-tuning has been demonstrated in capacitive vibration power generation [18], [19], [20], [21], [22] but has never been investigated in inductive vibration power generation.

In this study, we verified by analysis, simulation, and experiment how much frequency modulation and power generation can be achieved by R-tuning compared to conventional LCR-tuning. The results show that resonant frequency modulation can be achieved by R-tuning alone by inserting a fixed reactance element in series with an inductive vibrating generator element. Here, for simplicity, the reactance element is limited to capacitance, but the basic argument remains the same when the inductance is inserted where only the sign of the frequency modulation is inverted. We showed a tradeoff between the frequency modulation and the power maximization and obtained its analytical expressions, which were consistent with simulation and experiments. Furthermore, the figures of merit for the inductive power generating element to achieve both frequency modulation and power maximization were clarified. Finally, the frequency modulation by R-tuning was demonstrated in an experiment using actual power generation devices.

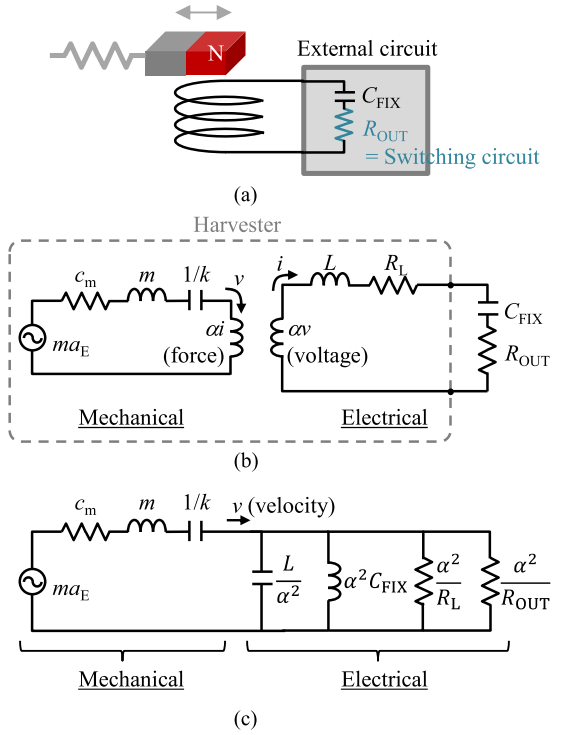

Fig. 1. (a) Model of inductive vibration energy harvester. (b) and (c) Equivalent circuits of the model. The vibrating magnet in (a) corresponds to "Mechanical" parts in (b) and (c). When we convert the electrical part in (b) to the mechanical counterpart, we obtain the equivalent circuit (c), which corresponds to (3).

II. Simulation

A model of inductive vibration energy harvesting is shown in Fig. 1(a). The relative vibration of the magnet and inductor generates an electromotive force, and the resulting power is extracted externally by a power extraction circuit (switching circuit) for use in a wireless circuit or to charge a battery. The switching circuit can be regarded as an average load resistance (R_{OUT}), the value of which can be varied by the switching frequency or the duty cycle in general [16]. The objective of this study is to enable the resonant frequency modulation via R_{OUT}, and the simplest method to achieve this is to insert a fixed capacitance (C_{FIX}) in series.

The generator element and the external circuit form an electromechanical coupling system [2], [3], which can be represented by the equivalent circuit shown in Fig. 1(b). The meanings of each constant and variable are summarized in Tables I and II, respectively. The coordinate X of the vibrating body is defined in relative coordinates that oscillate with the environmental vibration with acceleration $\sqrt{2}a_{\mathrm{E}}\sin(\omega t)$, and the mechanical force is also considered as an inertial force (ma_{E} in root mean square) in relative coordinates. Then the equation of motion of the vibrating body is given as follows:

$$m\sqrt{2}a_{\mathrm{E}}\sin(\omega t) = m\frac{d^2X}{dt^2} + c_{\mathrm{m}}\frac{dX}{dt} + kX + \alpha I. \quad (1)$$

TABLE I
List of Symbols

Property	Symbol	Unit
Mass position in the relative coordinate	X	m
Root mean square of mass velocity in the relative coordinate	v	ms^{-1}
Current in the external circuit	I	A
Root mean square of current in the external circuit	i	A
Time	t	s
Frequency of environmental vibration	f	Hz
Angular frequency of environmental vibration	ω	rad s^{-1}
Load resistance representing the switching circuit for power management	R_{OUT}	Ω
Inserted fixed capacitance	C_{FIX}	F

TABLE II
LIST OF CONSTANTS FOR SIMULATION AND EXPERIMENTS

Property	Symbol	Fig. 2–5 Sim.	Fig.6 and 7 EH13	Fig. 8 V-gen
Inertial mass	m	0.71 g	0.71 g	2.33 g
Spring stiffness	k	898 $N.m^{-1}$	898 $N.m^{-1}$	4110 $N.m^{-1}$
Mechanical damping	c_m	0.00476 $Ns.m^{-1}$	0.00476 $Ns.m^{-1}$	0.0978 $Ns.m^{-1}$
Coil inductance	L	0.575 H	0.023 H	0.69 H
Coil resistance	R_L	1.87 kΩ	374 Ω	270 Ω
Coupling coefficient	α	56.7 $Vs.m^{-1}$	11.3 $Vs.m^{-1}$	9.38 $Vs.m^{-1}$
Root mean square of environmental acceleration	a_E	0.2 ms^{-2}	0.2 ms^{-2}	1.0 ms^{-2}

The equation of the electrical circuit is given as follows:

$$\alpha \frac{dX}{dt} = L\frac{dI}{dt} + (R_L + R_{OUT})\, I + \frac{1}{C_{FIX}} \int I dt. \quad (2)$$

An electromotive force is generated in the electrical system in proportion to the speed in the mechanical system [left term of (2)], and a braking force is generated in the mechanical system in proportion to the current in the electrical system [last term of (1)]. By removing I from these two equations, we obtain the equivalent equation of motion of the vibrating body as follows:

$$ma_E = \left(c_m + i\omega m + \frac{k}{i\omega} + \frac{\alpha^2}{R_L + R_{OUT} + i\omega L + \frac{1}{i\omega C_{FIX}}} \right) v. \quad (3)$$

This equation of motion corresponds to the equivalent circuit, as shown in Fig. 1(c), where the electrical L is converted into a capacitive component L/α^2 in the mechanical counterpart, and the electrical C_{FIX} is converted into an inductive component $\alpha^2 C_{FIX}$ as well. Because this equivalent circuit in Fig. 1(c) covers all the mechanical–electrical interactions, it is easy to discuss impedance matching and to clarify the relationship between the amount of frequency modulation and the generated power.

Fig. 2(a) and (b) shows a simulation of the resonance characteristics when the values in Table II are assumed for the parameters of the vibration power generation element. When the vibration frequency is varied, the power consumed by the R_{OUT} (P_{OUT}) reaches its maximum at the resonance frequency. As shown by thin solid curves in Fig. 2(a), the resonant frequency varies depending on the value of R_{OUT}. As R_{OUT} decreases, the P_{OUT} peak falls once but rises again, and the envelope of P_{OUT} is characterized by two maxima [see bold curve in Fig. 2(a)]. The frequencies at the two maxima are almost equal to the resonance frequencies at open- and short-circuit conditions under some assumptions, as shown later (see explanations for Fig. 4). The

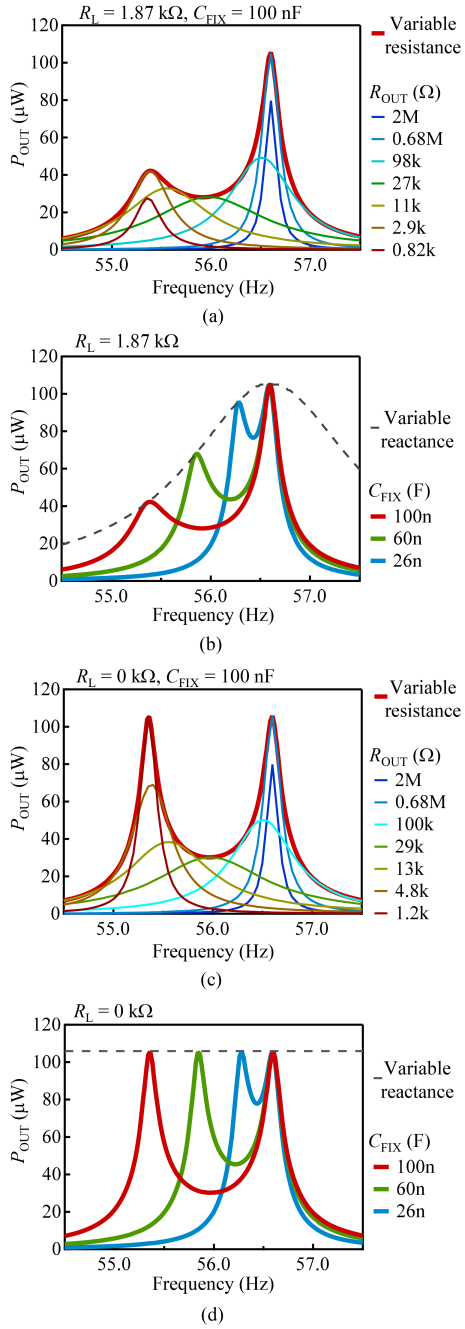

Fig. 2. (a) Simulated P_{OUT} as a function of vibration frequency for $R_L = 1.87$ kΩ. Each curve corresponds to different R_{OUT} with fixed $C_{FIX} = 100$ nF. (b) Simulated P_{OUT} with R-tuning for $R_L = 1.87$ kΩ and three different C_{FIX}. The dashed curve corresponds to the P_{OUT} with RC-tuning. (c) Simulated P_{OUT} for $R_L = 0$ Ω and different R_{OUT} values. (d) Simulated P_{OUT} with R-tuning for $R_L = 0$ Ω and three different C_{FIX}. The dashed line corresponds to the P_{OUT} with RC-tuning.

envelope of P_{OUT} is calculated by a resistive matching condition that matches only the absolute value of the impedance.

$$\frac{R_{OUT}}{\alpha^2} = \left| \frac{R_L}{\alpha^2} + i\left(\frac{L\omega}{\alpha^2} - \frac{1}{\alpha^2 C_{FIX}\omega} \right) + \left(c_m + i\left(m\omega - \frac{k}{\omega} \right) \right)^{-1} \right| \quad (4)$$

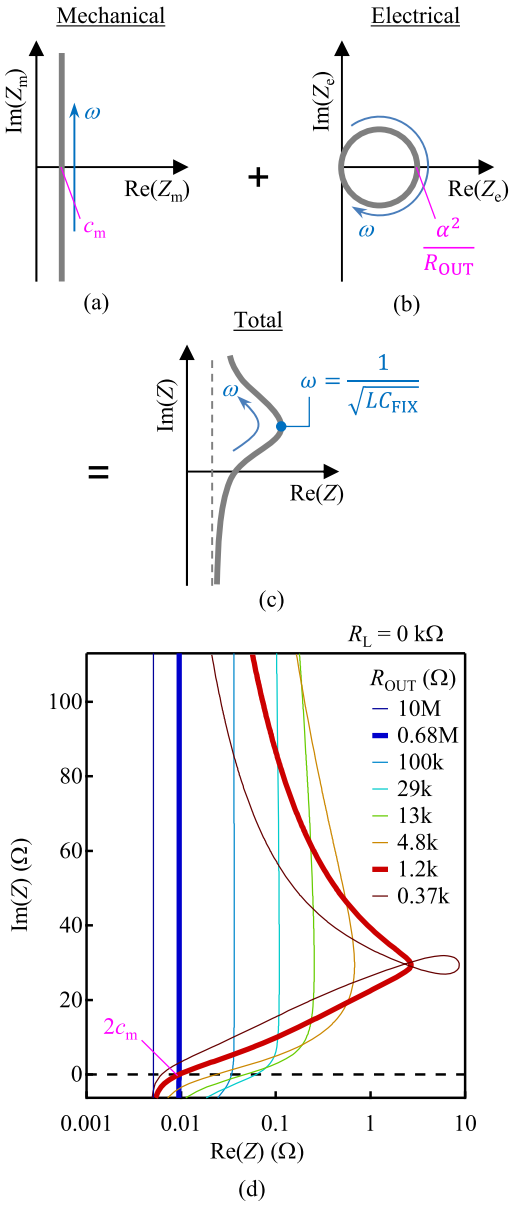

Fig. 3. (a)–(c) Schematic illustrations of impedance in the equivalent circuit of Fig. 1(c). (d) Simulated total impedance Z for different R_{OUT}.

$$P_{OUT} = \left| m a_E \frac{Z'_e}{Z_m + Z'_e} \right|^2 \frac{R_{OUT}}{\alpha^2} \tag{5}$$

$$Z_m = c_m + i\left(m\omega - \frac{k}{\omega}\right) \tag{6}$$

$$Z'_e = \left(\frac{R_L + R_{OUT}}{\alpha^2} + i\left(\frac{L\omega}{\alpha^2} - \frac{1}{\alpha^2 C_{FIX}\omega}\right)\right)^{-1}. \tag{7}$$

Equations (4) and (5) give the optimal R_{OUT} and P_{OUT} at each frequency, respectively. The left side of (4) is the effective admittance of the load resistance in the equivalent circuit of Fig. 1(c), and the right side is the absolute value of the complex admittance of the other parts. Thus, it is demonstrated that by

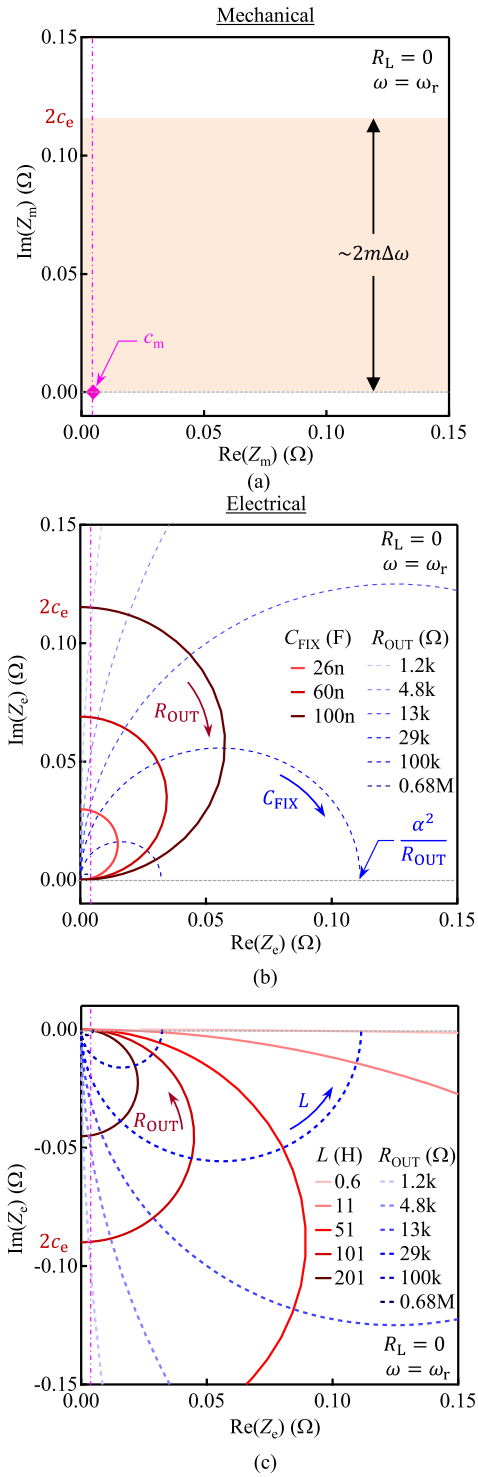

Fig. 4. (a) Mechanical impedance Z_m at $\omega = \omega_r$. (b) Equivalent electrical impedance Z_e at $\omega = \omega_r$ for various R_{OUT} and C_{FIX}. (c) Z_e at $\omega = \omega_r$ for various R_{OUT} and L as a reference.

inserting C_{FIX}, the resonance frequency can be modulated only by R-tuning. It should be noted that the insertion of the fixed reactance component (C_{FIX}) is indispensable for frequency modulation; otherwise, the R-tuning only modifies the dumping constant of resonance, as obvious in Fig. 1(c), if the parasitic L is too small to be counted as the fixed reactive component.

In *R*-tuning, the two frequencies at which P_{OUT} reaches its local maximum depend on C_{FIX}, and the larger the C_{FIX} is, the more separated these peak frequencies become [see Fig. 2(b)]. Therefore, the larger C_{FIX} leads to the larger frequency modulation, but at the same time, it also leads to the smaller P_{OUT} with tradeoff. The envelope of P_{OUT} for various C_{FIX} values [see dashed curve in Fig. 2(b)] corresponds to the curve of P_{OUT} optimized by *RC*-tuning, as previously reported [10], [14], and this curve satisfies the complex impedance matching condition.

$$\frac{R_{\mathrm{OUT}}}{\alpha^2} = \mathrm{Re}\left[\frac{R_{\mathrm{L}}}{\alpha^2} + i\left(\frac{L\omega}{\alpha^2} - \frac{1}{\alpha^2 C_{\mathrm{FIX}}\omega}\right) + \left(c_{\mathrm{m}} + i\left(m\omega - \frac{k}{\omega}\right)\right)^{-1}\right] \tag{8}$$

$$0 = \mathrm{Im}\left[\frac{R_{\mathrm{L}}}{\alpha^2} + i\left(\frac{L\omega}{\alpha^2} - \frac{1}{\alpha^2 C_{\mathrm{FIX}}\omega}\right) + \left(c_{\mathrm{m}} + i\left(m\omega - \frac{k}{\omega}\right)\right)^{-1}\right]. \tag{9}$$

From these two equations, R_{OUT} and C_{FIX} are uniquely determined for each ω, and P_{OUT} is calculated as the dashed curve in Fig. 2(b). In other words, the tradeoff between the resonance frequency modulation and the P_{OUT} maximization in *R*-tuning is essentially the same tradeoff as the previously reported *RC*-tuning. The difference in *R*-tuning from the previously reported *RC*-tuning is that at frequencies between the two maxima, the complex impedance matching conditions (8) and (9) are not satisfied, so P_{OUT} is slightly decreased. In such a case, the higher P_{OUT} can be maintained by changing C_{FIX} discretely, as shown by bold curves in Fig. 2(b), which is a realistic solution for small power generators.

The reason why P_{OUT} decreases as the resonant frequency is modulated is that the matched R_{OUT} becomes smaller and the resistive loss at R_{L} becomes comparatively larger. In other words, R_{L} is one of the main factors that determine the limit of frequency modulation, as was also pointed out in *RC*-tuning previously [10], [14]. In fact, assuming $R_{\mathrm{L}} = 0$, (8) and (9) become simple impedance matching conditions between the electrical and mechanical systems, and P_{OUT} does not decrease for resonant frequency modulation [dashed line in Fig. 2(d)].

$$P_{\mathrm{OUT-MAX}} = \frac{(ma_{\mathrm{E}})^2}{4c_{\mathrm{m}}}. \tag{10}$$

This equation is valid under the condition of constant vibration acceleration of the environment. It should be noted that the prior literature [10], [14] assumes constant vibrational displacement of the environment (not constant acceleration), where a_{E} and $P_{\mathrm{OUT\text{-}MAX}}$ are proportional to f^2 and f^4, respectively. It should also be noted that in Fig. 2(d), the two frequencies at P_{OUT} maxima for *R*-tuning [see bold curves in Fig. 2(d)] are rigorously given by two solutions of (8) and (9) when C_{FIX} is a constant and ω is a variable. Interestingly, in piezoelectric energy harvesting, P_{OUT} also shows similar double peak characteristics for *R*-tuning, which has been used for resonance frequency modulation [18], [19], [20], [21], [22]. In that case, the capacitance of the piezoelectric device is relatively large and can be regarded as the fixed reactance element, corresponding to C_{FIX} in our study. The essential difference of our inductive power generator from the piezoelectric power generator is the existence of nonnegligible R_{L} and the relatively weak mechanical–electrical coupling.

III. Analysis of Frequency Modulation

To investigate the upper limit of resonant frequency modulation in *R*-tuning, we consider the complex impedance of the entire electromechanical coupling system in Fig. 1(c). Here, we discuss the case $R_{\mathrm{L}} = 0$, which is intuitively easy to understand and use it as a reference for the case $R_{\mathrm{L}} \neq 0$. First, the complex impedance of the mechanical system is expressed by the following equation, and in the complex impedance plane, it is a straight line with respect to the frequency change, as shown in Fig. 3(a):

$$Z_{\mathrm{m}} = c_{\mathrm{m}} + i\left(m\omega - \frac{k}{\omega}\right). \tag{11}$$

The complex impedance of the electrical system converted into the mechanical impedance is expressed by the following equation, which is a circle of diameter $\alpha^2/R_{\mathrm{OUT}}$ with respect to frequency change, as shown in Fig. 3(b):

$$Z_{\mathrm{e}} = \left(\frac{R_{\mathrm{OUT}}}{\alpha^2} + i\left(\frac{L\omega}{\alpha^2} - \frac{1}{\alpha^2 C_{\mathrm{FIX}}\omega}\right)\right)^{-1}. \tag{12}$$

These are added together to form the complex impedance of the coupled system, and the curve bulges out in the real axis direction, as shown in Fig. 3(c)

$$Z = Z_{\mathrm{m}} + Z_{\mathrm{e}}. \tag{13}$$

The smaller the R_{OUT}, the larger the electrical impedance circle becomes, and the steeper the bulge of *Z* becomes in the real axis direction. The actual simulation of *Z* for various R_{OUT} values is shown in Fig. 3(d). It can be seen that when R_{OUT} is large, *Z* is almost straight, but as R_{OUT} goes down, it curves greatly and bulges in the direction of the real axis.

When the complex impedance is matched between the electrical and mechanical systems, the total impedance is given by $Z = 2c_{\mathrm{m}}$, which is a real number. Therefore, we focus on the point where *Z* intersects the real axis in Fig. 3(d). We can see that initially for small R_{OUT}, the intersect is close to c_{m} (curve for 0.37 kΩ), but as R_{OUT} increases, it moves to the right (curves for 13 and 29 kΩ) and then moves back and returns to $Z = c_{\mathrm{m}}$ again (curve for 10 MΩ). As a result, the condition of complex impedance matching ($Z = 2c_{\mathrm{m}}$) is satisfied twice [bold curves in Fig. 3(d)], resulting in double-peak characteristics in P_{OUT}.

Then, the double peak frequencies in *R*-tuning can be approximately obtained as follows. Let $\omega_{\mathrm{r}} = \sqrt{k/m}$ be the resonant frequency when the circuit terminals are open. Fig. 4(a) and (b) shows Z_{m} and Z_{e} at $\omega = \omega_{\mathrm{r}}$. For the mechanical system, $Z_{\mathrm{m}} = c_{\mathrm{m}}$, represented by the pink dot in Fig. 4(a). For the electrical system, Z_{e} draws a semicircle centered on the imaginary axis for changes in R_{OUT} (*R*-tuning, red solid curve) and a circular arc centered on the real axis for changes in C_{FIX} (blue dashed curve), as shown in Fig. 4(b). The radius c_{e} of the

semicircle for *R*-tuning is given as follows:

$$c_{\mathrm{e}} = \frac{\alpha^2}{2\left(\frac{1}{C_{\mathrm{FIX}}\omega_{\mathrm{r}}} - L\omega_{\mathrm{r}}\right)}. \tag{14}$$

For simplicity, we assume $\frac{1}{C_{\mathrm{FIX}}\omega_{\mathrm{r}}} - L\omega_{\mathrm{r}} > 0$. The opposite case can also be understood as the resonant frequency modulation by inserting a fixed inductance instead of a fixed C_{FIX}. In this case, Z_{e} for various R_{OUT} and L are plotted in Fig. 4(c), where L values are so large that insertion of an extra inductance is inappropriate for resonant frequency modulation in the current device. As is clear from Fig. 4(b), Z_{e} intersects the line $\mathrm{Re}\ (Z_{\mathrm{e}}) = c_{\mathrm{m}}$ twice for *R*-tuning as long as $c_{\mathrm{e}} > c_{\mathrm{m}}$. Then, at each intersection, the condition for complex impedance matching can be satisfied by changing ω until Z_{m} satisfies $\mathrm{Im}\ (Z_{\mathrm{m}}) = -\mathrm{Im}(Z_{\mathrm{e}})$. Here, it is assumed that the change of Z_{e} with respect to ω is negligible, which is a reasonable approximation as explained later [see (21)]. First, the R_{OUT} at this intersection between the Z_{e} semicircle and the line $\mathrm{Re}\ (Z_{\mathrm{e}}) = c_{\mathrm{m}}$ is given as follows:

$$R_{\mathrm{OUT}\pm} = \frac{\alpha^2}{2c_{\mathrm{m}}}\left(1 \pm \sqrt{1 - \left(\frac{c_{\mathrm{m}}}{c_{\mathrm{e}}}\right)^2}\right). \tag{15}$$

And since $\mathrm{Im}(Z_{\mathrm{e}})$ at this intersection corresponds to the amount of resonance frequency modulation from ω_{r}, the resonance frequencies at the double peaks of *R*-tuning are given by the following equation:

$$\omega_{\pm} = \omega_{\mathrm{r}} - \frac{c_{\mathrm{m}}}{2m}\sqrt{\frac{\alpha^2}{c_{\mathrm{m}}R_{\mathrm{OUT}\pm}} - 1}. \tag{16}$$

The inside of the root of (16) can be shown always positive. Note that $\frac{c_{\mathrm{m}}}{2m}$ in (16) is the full-width at half-maximum (FWHM) of P_{OUT} with respect to ω when R_{OUT} is sufficiently large. Therefore, (16) indicates that $c_{\mathrm{m}}R_{\mathrm{OUT}-} \ll \alpha^2$ is required to sufficiently shift ω_- from ω_{r} compared to the FWHM. This condition is satisfied as long as $c_{\mathrm{e}} \gg c_{\mathrm{m}}$. On the other hand, ω_+ cannot be significantly shifted from ω_{r} when $c_{\mathrm{e}} \gg c_{\mathrm{m}}$, according to (15) and (16). Then, $\Delta\omega = \omega_+ - \omega_- \approx \omega_{\mathrm{r}} - \omega_-$ is the frequency difference between the double peaks in *R*-tuning, which gives a measure of frequency modulation for each C_{FIX} value. It is clear from Fig. 4(b) that the imaginary components of the intersection of the Z_{e} semicircle and the line $Re\ (Z_{\mathrm{e}}) = c_{\mathrm{m}}$ are almost identical to the imaginary components of the points at $R_{\mathrm{OUT}} = 0, \infty$ (intercepts of the imaginary axis). This means that $\omega_{\pm}$ is close to the resonance frequencies when the circuit terminals are opened and shorted, respectively, as pointed out in the past literature [22].

Using the above discussion of the $R_{\mathrm{L}} = 0$ case as a basis, we consider the case where $R_{\mathrm{L}} \neq 0$. If the impedance matching between the electrical and mechanical systems is considered as an approximation instead of the impedance matching between R_{OUT} and the rest part, similar equations to (15) and (16) are obtained by replacing $R_{\mathrm{OUT}\pm}$ with $R_{\mathrm{L}} + R_{\mathrm{OUT}\pm}$. From (16), it can be seen that $R_{\mathrm{OUT}-}$ must be small enough to satisfy $c_{\mathrm{m}}(R_{\mathrm{L}} + R_{\mathrm{OUT}-}) \ll \alpha^2$ in order to modulate ω_- from ω_{r} meaningfully. On the other hand, since P_{OUT} is proportionally divided by R_{L} and $R_{\mathrm{OUT}-}$, $R_{\mathrm{OUT}-}$ shouldn't be too small with respect to R_{L}. Therefore, in order to maximize frequency modulation while maintaining P_{OUT}, an optimal C_{FIX} has to be selected such that $R_{\mathrm{OUT}-} = R_{\mathrm{L}}$, and the corresponding ω_- gives a rough estimate of the maximum modulation of the resonant frequency. The maximum $\Delta\omega$ and the corresponding C_{FIX} are estimated as follows from (16):

$$\Delta\omega \approx \frac{\omega_{\mathrm{r}}}{2Q}\frac{\alpha}{\sqrt{2R_{\mathrm{L}}c_{\mathrm{m}}}} = \frac{\omega_{\mathrm{r}}}{2}\sqrt{\frac{c_{\mathrm{m}}}{mk}}\sqrt{\frac{\alpha^2}{2R_{\mathrm{L}}}} \tag{17}$$

$$\frac{1}{C_{\mathrm{FIX}}\omega_{\mathrm{r}}} - L\omega_{\mathrm{r}} \approx \sqrt{\frac{2\alpha^2R_{\mathrm{L}}}{c_{\mathrm{m}}}}. \tag{18}$$

Q is the Q value of the mechanical resonance when the external circuit terminals are open, $Q = \sqrt{mk}/c_{\mathrm{m}}$. When this $\Delta\omega$ is achieved, $P_{\mathrm{OUT\text{-}MAX}}$ in (10) is divided into half by R_{L} and $R_{\mathrm{OUT}-}$. Precisely, however, this value of P_{OUT} is derived from the impedance matching between the electrical system and the mechanical system, and if the impedance matching of R_{OUT} alone is considered, the peak value of P_{OUT} is slightly larger, and $R_{\mathrm{OUT}-}$ at that peak becomes smaller than R_{L}.

From (17), it can be seen that small R_{L} and large α are preferable for the frequency modulation. On the other hand, large c_{m} and small m leads not only to the large modulation but also to small P_{OUT} according to (10). In other words, it is not recommended to vary c_{m} and m for the purpose of resonant frequency modulation. To disentangle this tradeoff from the ability of resonant frequency modulation for each device, we can define the following absolute figure of merit (AFOM) from the last term in (17):

$$\mathrm{AFOM} = \sqrt{\frac{\alpha^2}{2R_{\mathrm{L}}}} = 4\Delta\omega\sqrt{\frac{P_{\mathrm{OUT\text{-}MAX}}}{a_{\mathrm{E}}^2}}. \tag{19}$$

This AFOM shows that the larger the coupling constant α and the smaller the winding resistance R_{L} of the coil, the larger the AFOM becomes, namely, the more suitable the element is for resonant frequency modulation. And the machine parameters c_{m}, m, and k only move $\Delta\omega$ and P_{OUT} up and down in opposite directions, respectively, and it is appropriate to separate them from the AFOM of the harvester element. Ideally, the vibration power generator should be designed to have small size and large AFOM.

On the other hand, even for the same $\Delta\omega$, shifting the steep resonance peak is of much greater practical value than shifting the broad resonance peak. Therefore, it is also meaningful how large $\Delta\omega$ can be made relative to the FWHM of the resonance peak at an open-circuit condition $\frac{c_{\mathrm{m}}}{2m}\left(=\frac{\omega_{\mathrm{r}}}{2Q}\right)$.

$$\mathrm{RFOM} = \frac{\Delta\omega}{\omega_{\mathrm{r}}/(2Q)} = \frac{\alpha}{\sqrt{2R_{\mathrm{L}}c_{\mathrm{m}}}} = \frac{\mathrm{AFOM}}{\sqrt{c_{\mathrm{m}}}}. \tag{20}$$

This relative figure of merit (RFOM) can be regarded as a "gain" of frequency bandwidth by electrical tuning. In other words, while the AFOM tells you the potential magnitude of

TABLE III
COMPARISON WITH THE PREVIOUS WORKS

	[10]	[14]	EH13	V-generator
m (g)	22	21.4	0.71	2.33
k (N.m^{-1})	3371	3220	898	4110
c_m (Ns.m^{-1})	0.345	0.31	0.00476	0.0978
α (Vs.m^{-1})	5.64	5.6	11.3	9.38
L (mH)	0.25	0.2	23	690
R_L (Ω)	1.6	3.3	374	270
$\Delta\omega$ by tuning (at half P_{OUT}) (rad.s^{-1})	39	38	2.5	1.9
FWHM of P_{OUT} (rad.s^{-1})	7.8	7.2	0.34	2.3
AFOM	**3.0**	**2.9**	**0.51**	**(0.25)**
Theoretical *AFOM*	2.7	2.2	0.41	0.42
RFOM	**5.0**	**5.2**	**7.5**	**(0.81)**
Theoretical *RFOM*	4.6	3.9	6.0	1.3
Normalized P_{OUT} at a_E = 1 ms^{-2} [mW/(ms^{-2})]	**0.36**	**0.38**	**2.6**	**1.1**

frequency modulation by maintaining P_{OUT}, the RFOM value indicates the benefit of electrical modulation.

If the RFOM of the power generating element is small, then, in principle, no meaningful electrical frequency modulation can be expected. In fact, (15) and (16) pointed out that meaningful frequency modulation can only be achieved if $c_e \gg c_m$. By substituting c_e with (14) and using the definition of RFOM [see (20)], this leads to the condition RFOM $\gg 2$. If RFOM < 2, there is no complex impedance matching solution as in (15), and modulating the resonance frequency while maintaining reasonable P_{OUT} becomes difficult. In other words, a mechanical method is suitable for modulating the resonant frequency of a generating element with RFOM < 2. Thus, by examining the RFOM of the harvester device, the appropriate frequency modulation method can be predicted. For electrical frequency modulation, the harvester device must be designed to make α large and make R_L and c_m small.

Table III lists benchmarks of AFOM and RFOM for electrical resonant frequency modulation. It can be seen that the generating device used in the experiments in this article described in the following ("EH13" in Table III) has a relatively low AFOM but a higher RFOM than the previous works. The reason why RFOM is higher in our device is because the damping coefficient of the mechanical resonance is much smaller, and hence, the original mechanical bandwidth is much narrower. The advantage

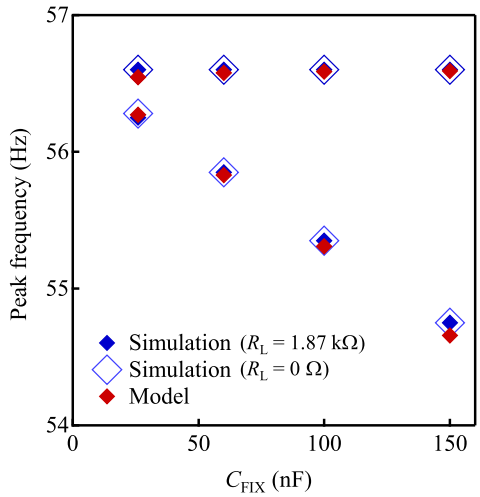

Fig. 5. P_{OUT} peak frequencies for R-tuning with various C_{FIX}. "Model" is calculated by (16).

of the narrower mechanical bandwidth is a larger P_{OUT}. Indeed, despite the size of EH13 (3.2 × 3.3 × 1.0 cm^3) being tens of times smaller than in the literature [10], [14], the P_{OUT} normalized by a_E = 1 ms^{-2} for EH13 is several times larger, as given in Table III. It should be noted that the small device size causes thinner coil windings (large R_L) or fewer turns (small α), which inevitably lead to smaller AFOM according to (19). In practice, generators require multifaceted comparison that includes AFOM, RFOM, device size, normalized P_{OUT}, etc. AFOM, RFOM, and normalized P_{OUT} are made bold in Table III.

Equations (16) and (17) are approximations neglecting the change of Z_e with respect to ω as mentioned above. We show that this approximation holds as long as the AFOM and RFOM values are not too large (the coupling is not so strong). The condition that the change of Z_e can be neglected with respect to the change of Z_m in the vicinity of $\omega = \omega_r$ is given by the following equation:

$$\left|\frac{dZ_e}{d\omega}\right|_{\omega=\omega_r} \ll \left|\frac{dZ_m}{d\omega}\right|_{\omega=\omega_r}. \tag{21}$$

Since Z_e hardly changes when $R_{OUT} = R_{OUT+}$, we limit ourselves to $R_{OUT} = R_{OUT-}$ to investigate the conditions under which this equation holds. Using (15), (21) becomes the following inequality:

$$\frac{c_m}{C_{FIX}\omega_r^2 R_{OUT-}} \ll m. \tag{22}$$

Replacing R_{OUT-} by $2R_L$ as described earlier to estimate the maximum $\Delta\omega$, and further assuming $2R_L c_m \ll \alpha^2$ as explained in (16), (21) [and (18)] becomes as follows:

$$Q \gg \frac{\alpha}{\sqrt{2R_L c_m}} \left(= \text{RFOM}\right). \tag{23}$$

Therefore, (21) is valid if the RFOM of the generating element is not too large. As a rough guide, substituting (17) into this equation yields $\omega_r/2 \gg \Delta\omega$, which means that (21) does not

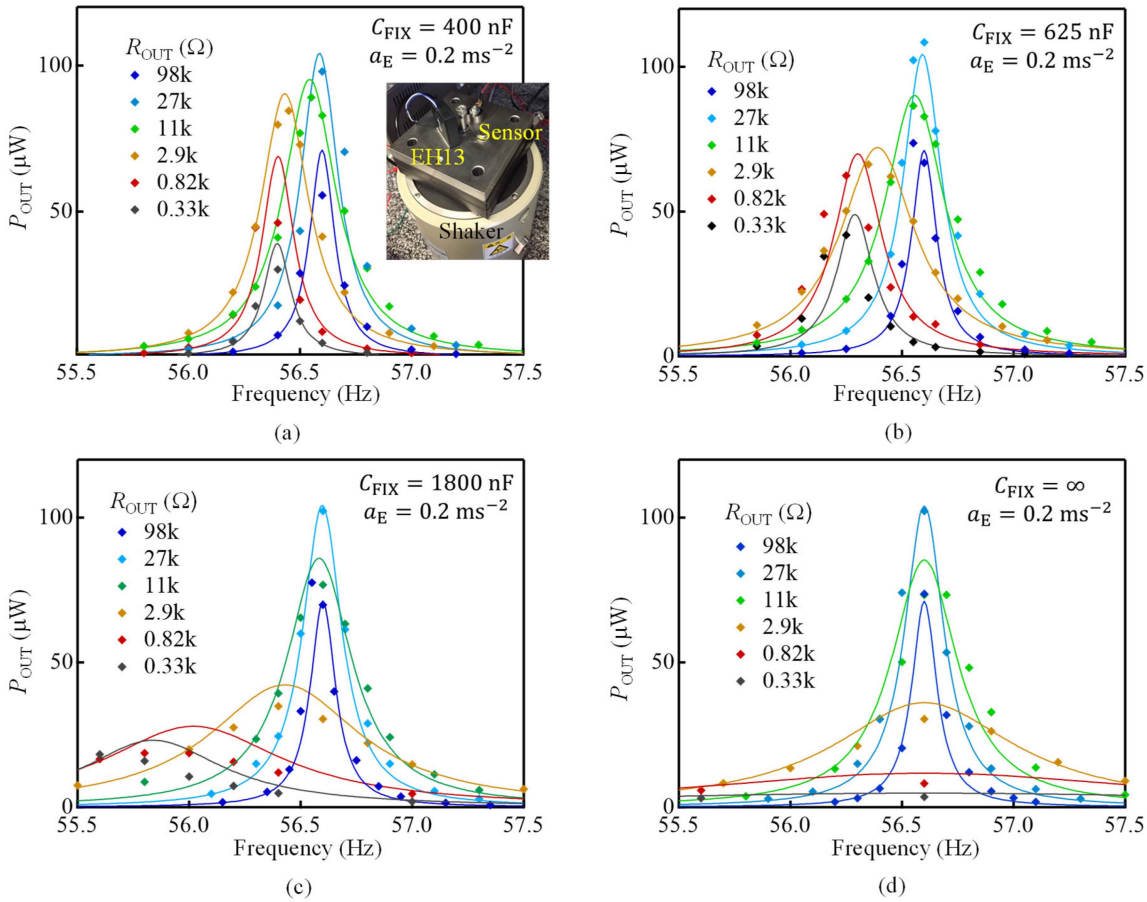

Fig. 6. P_{OUT} versus frequency for different R_{OUT} values with (a) $C_{FIX} = 400$ nF, (b) $C_{FIX} = 625$ nF, (c) $C_{FIX} = 1800$ nF, and (d) $C_{FIX} = \infty$. Markers represent experiments and curves represent simulation by (3). The inset in (a) is the experimental setup.

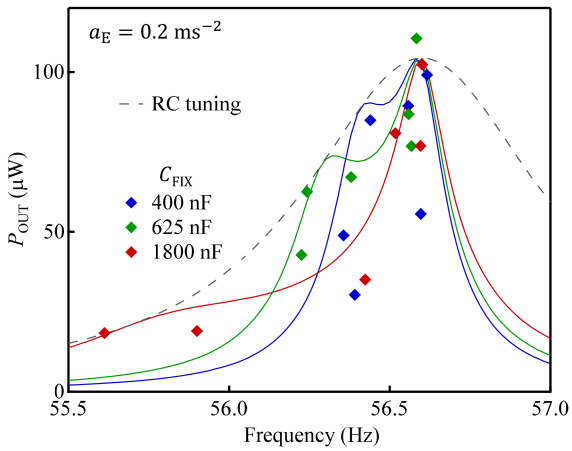

Fig. 7. Experimentally obtained frequency and P_{OUT} at the resonant peaks in Fig. 6 for different R_{OUT} and C_{FIX}. The solid curves and the dashed curve show simulated P_{OUT} for R-tuning [see (4) and (5)] and RC-tuning [see (8) and (9)], respectively.

hold if $\Delta\omega$ is comparable to ω_r. Equation (21) is correct in most cases for small vibration power generators. In fact, (21) is valid for all the generators in Tables II and III. For example, as for the generator ("Sim.") in Table II, (16) and (17) are indeed in good agreement with the simulation results in Fig. 2. To show this, Fig. 5 plots the resonance frequencies $\omega_\pm/(2\pi)$ for R-tuning against C_{FIX}. It shows that $\omega_\pm/(2\pi)$ obtained from (16) is almost consistent with the value obtained in simulation. Furthermore, ω_- is hardly affected by the fact that $R_L \neq 0$. This is because as long as $c_e \gg c_m$, ω_- almost matches the resonance frequency when the circuit terminals are shorted.

IV. Experimental Demonstration

Finally, resonance frequency modulation by R_{OUT} was experimentally demonstrated. EH13 (Toyo Electronics Corporation) is a vibration energy harvester with extremely small mechanical dumping, specialized for high P_{OUT} and narrow bandwidth (see Table II). In the experiment, it was fixed to the stage with an accelerometer, and the stage was vibrated by a shaker at a constant acceleration of 0.2 ms^{-2} root mean square, as shown in the inset of Fig. 6(a). Fig. 6(a)–(c) shows the R-tuning of the resonant frequencies when C_{FIX} was fixed at 400 nF, 625 nF, and 1800 nF, respectively. Fig. 6(b) for $C_{FIX} = 625$ nF corresponds to the maximum modulation condition of (18). The experimental data (diamond mark) are in close agreement with the simulation results (curve), indicating that resonance frequency modulation

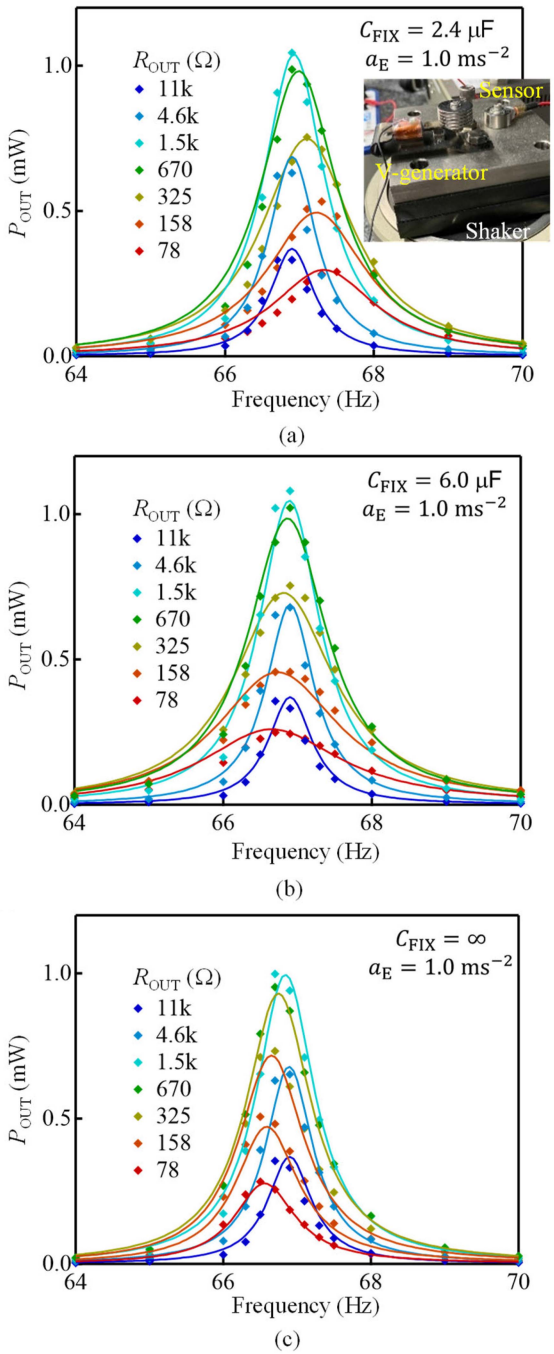

Fig. 8. P_{OUT} versus frequency for different R_{OUT} values with (a) C_{FIX} = 2.4 μF, (b) C_{FIX} = 6.0 μF, and (c) $C_{FIX} = \infty$ in the V-generator device. Markers represent experiments and curves represent simulation by (3). The inset in (a) is the experimental setup.

is successfully demonstrated by *R*-tuning. As a comparison, the *R*-tuning without C_{FIX} does not show any change in resonance frequency, as shown in Fig. 6(d), where $C_{FIX} = \infty$ means the capacitance is removed and electrically shorted. This is because, as shown in Fig. 4(b), it is essential to insert C_{FIX} and make c_e large in order to achieve frequency modulation. All the resonant peaks in Fig. 6 are summarized as P_{OUT} versus frequency in Fig. 7. The experimental values (diamonds in Fig. 7) are approximately consistent with the simulated P_{OUT} curves for *R*-tuning (solid curves) and *RC*-tuning (dashed curve).

As another demonstration, the V-generator ("Medium size," Kanazawa University, Japan), a vibration power generation device using magnetostrictive materials [3], [23], was used, as shown in Fig. 8. The V-generator is a small-sized high-power vibration power generation device (see Table II) that can accommodate large *m* and *k* in its compact structure (2.4 × 6.7 × 2.1 cm^3). Although the normalized output power is not as large as EH13, the mechanical bandwidth is almost an order of magnitude larger. Despite the excellent device characteristics, the resonance frequency is only slightly reduced by *R*-tuning, as shown in Fig. 8(a), even if an appropriate C_{FIX} calculated by (18) is connected to this generator element. Furthermore, since the P_{OUT} is simultaneously reduced by frequency modulation, there is little benefit from frequency modulation when compared to the curve for $R_{OUT} = 1.5$ kΩ in Fig. 8(a). Further increase in C_{FIX} does not produce any improvement, as shown in Fig. 8(b). When C_{FIX} is removed and shorted ($C_{FIX} = \infty$), the large *L* of the V-generator causes *R*-tuning in the direction of increasing resonant frequency, as shown in Fig. 8(c), but the modulation is still small and does not provide a significant advantage over the curve with $R_{OUT} = 1.5$ kΩ.

The reason why the V-generator does not provide a meaningful modulation effect is because of its small RFOM, as given in Table III. In fact, the theoretical RFOM of the V-generator does not satisfy the condition $RFOM \gg 2$, so electrical frequency modulation is not suitable in principle. In this case, mechanical frequency modulation is more suitable. Thus, by calculating the RFOM of each vibration power generator, the optimal method for resonant frequency modulation can be identified. In Table III, the experimental values of AFOM and RFOM for the V-generator are put in parentheses because the conditions necessary for their definitions ($c_e > c_m$) are not satisfied, and hence, they are only the nominal values.

It should be noted that the equations of motion for the capacitive vibration power generator are qualitatively the same as those for the inductive vibration power generator. The critical difference is that in the case of a capacitive generator, the resonant frequency modulation is determined by the capacitance of the power generation device, which sets the maximum of C_{FIX} [18], rather than by the resistive component such as R_L. Therefore, the AFOM and the RFOM as the functions of R_L in this article are specific to inductive devices and do not apply to capacitive devices. By the way, frequency modulation in the reverse direction is possible by inserting an inductance in series, as demonstrated in a capacitive power generator [19]. In this case, however, a new winding resistance is created, which limits the amount of frequency modulation, and sometimes, the inductance necessary for frequency modulation becomes too large, as demonstrated in Fig. 4(c).

V. Conclusion

We have shown that, in inductive oscillatory power generation, the resonant frequency can be changed only by *R*-tuning by inserting a fixed reactance element in series with the power

circuit. Two types of figures of merit, one indicating the magnitude of frequency modulation and the other indicating its gain with respect to the original bandwidth, can be defined for each energy harvester device by the winding resistance of the generator coil, the mechanical dumping constant, and the electromechanical coupling coefficient. Especially, the second figure of merit, denoted as "RFOM," tells whether the specific harvester device is suitable for electrical frequency modulation or for mechanical frequency modulation. We also experimentally demonstrated resonant frequency modulation by *R*-tuning using actual vibrating power generation devices. This research will enhance the versatility of inductive vibration power generation elements, which have been increasingly applied in recent years, and provide a basis for their application in a wide range of industries.

ACKNOWLEDGMENT

The author would like to thank K. Takeuchi at the NTT Data Institute of Management Consulting, Inc., K. Ishino and engineers at Toyo Electronics Corporation, Prof. T. Ueno, Prof. S. Kita, and Dr. T. Minamitani at Kanazawa University for energy harvesting devices.

REFERENCES

[1] S. P. Beeby, M. J. Tudor, and N. M. White, "Energy harvesting vibration sources for microsystems applications," *Meas. Sci. Technol.*, vol. 17, pp. R175–R195, Oct. 2006, doi: 10.1088/0957-0233/17/12/R01.

[2] S. Cheng, N. Wang, and D. P. Arnold, "Modeling of magnetic vibrational energy harvesters using equivalent circuit representations," *J. Micromech. Microeng.*, vol. 17, pp. 2328–2335, Oct. 2007, doi: 10.1088/0960-1317/17/11/021.

[3] S. Kita, T. Ueno, and S. Yamada, "Improvement of force factor of magnetostrictive vibration power generator for high efficiency," *J. Appl. Phys.*, vol. 117, Feb. 2015, Art. no. 17B508, doi: 10.1063/1.4907237.

[4] E. Lefeuvre, D. Audigier, C. Richard, and D. Guyomar, "Buck-boost converter for sensorless power optimization of piezoelectric energy harvester," *IEEE Trans. Power Electron.*, vol. 22, no. 5, pp. 2018–2025, Sep. 2007, doi: 10.1109/TPEL.2007.904230.

[5] D. Guyomar and M. Lallart, "Recent progress in piezoelectric conversion and energy harvesting using nonlinear electronic interfaces and issues in small scale implementation," *Micromachines*, vol. 2, no. 2, pp. 274–294, Jun. 2011, doi: 10.3390/mi2020274.

[6] J. Boland, Y.-H. Chao, Y. Suzuki, and Y. C. Tai, "Micro electret power generator," in *Proc. 16th Annu. Int. Conf. Micro Electro Mech. Syst.*, 2003, pp. 538–541, doi: 10.1109/MEMSYS.2003.1189805.

[7] H. Honma, Y. Tohyama, and H. Toshiyoshi, "A paradoxical approach to enhance the output power of vibrational energy harvester beyond the impedance matching conditions," in *Proc. IEEE 33rd Int. Conf. Micro Electro Mech. Syst.*, 2020, pp. 594–597, doi: 10.1109/MEMSYS.2003.1189805.

[8] Y. Liu, A. Badel, and Y. Suzuki, "Enhancing output power of rotational electret energy harvester by synchronized switch harvesting on inductor," *J. Intell. Mater. Syst. Struct.*, vol. 33, no. 1, pp. 1–13, May 2021, doi: 10.1177/1045389X211011676.

[9] Y. Li, C. Zhou, X. Wang, J. Wang, D. Qiao, and K. Tao, "A vibration energy harvester with targeted frequency-tuning capability," *IEEE Trans. Instrum. Meas.*, vol. 71, 2022, Art. no. 7503010, doi: 10.1109/TIM.2022.3175984.

[10] A. Cammarano, S. G. Burrow, D. A. W. Barton, A. Carrella, and L. R. Clare, "Tuning a resonant energy harvester using a generalized electrical load," *Smart Mater. Struct.*, vol. 19, Mar. 2010, Art. no. 055003, doi: 10.1088/0964-1726/19/5/055003.

[11] P. D. Mitcheson, T. T. Toh, K. H. Wong, S. G. Burrow, and A. S. Holmes, "Tuning the resonant frequency and damping of an electromagnetic energy harvester using power electronics," *IEEE Trans. Circuits Syst. II, Exp. Briefs*, vol. 58, no. 12, pp. 792–796, Dec. 2011, doi: 10.1109/TCSII.2011.2173966.

[12] D. Zhu, S. Roberts, T. Mouille, M. J. Tudor, and S. P. Beeby, "General model with experimental validation of electrical resonant frequency tuning of electromagnetic vibration energy harvesters," *Smart Mater. Struct.*, vol. 21, Sep. 2012, Art. no. 105039, doi: 10.1088/0964-726/21/10/105039.

[13] D. Mallick and S. Roy, "Bidirectional electrical tuning of FR4 based electromagnetic energy harvesters," *Sensors Actuators A, Phys.*, vol. 226, pp. 154–162, May 2015, doi: 10.1016/j.sna.2015.02.016.

[14] J. A. Bowden, S. G. Burrow, A. Cammarano, L. R. Clare, and P. D. Mitcheson, "Switched-mode load impedance synthesis to parametrically tune electromagnetic vibration energy harvesters," *IEEE/ASME Trans. Mechatronics*,, vol. 20, no. 2, pp. 603–610, Apr. 2015, doi: 10.1109/TMECH.2014.2325825.

[15] H. Zhang, L. R. Corr, and T. Ma, "Effects of electrical loads containing non-resistive components on electromagnetic vibration energy harvester performance," *Mech. Syst. Signal Process.*, vol. 101, pp. 55–66, Feb. 2018, doi: 10.1016/j.ymssp.2017.08.031.

[16] G. D. Szarka, S. G. Burrow, P. P. Proynov, and B. H. Stark, "Maximum power transfer tracking for ultralow-power electromagnetic energy harvesters," *IEEE Trans. Power Electron.*, vol. 29, no. 1, pp. 201–212, Jan. 2014, doi: 10.1109/TPEL.2013.2251427.

[17] H. Xiao, H. Peng, X. Liu, and H. Sun, "Fully self-powered inductorless electromagnetic vibration energy harvesting system using auxiliary coils for hysteresis current MPPT control," *IEEE Trans. Power Electron.*, vol. 37, no. 11, pp. 13192–13204, Nov. 2022, doi: 10.1109/TPEL.2022.3182155.

[18] Y. Liao and H. A. Sodano, "Optimal parameters and power characteristics of piezoelectric energy harvesters with an *RC* circuit," *Smart Mater. Struct.*, vol. 18, Mar. 2009, Art. no. 045011, doi: 10.1088/0964-1726/18/4/045011.

[19] J. M. Renno, M. F. Daqaqb, and D. J. Inman, "On the optimal energy harvesting from a vibration source," *J. Sound Vib.*, vol. 320, no. 1/2, pp. 386–405, Feb. 2009, doi: 10.1016/j.jsv.2008.07.029.

[20] A. Badel and E. Lefeuvre, "Wideband piezoelectric energy harvester tuned through its electronic interface circuit," *J. Phys., Conf. Ser.*, vol. 557, Nov. 2014, Art. no. 012115, doi: 10.1088/1742-6596/557/1/012115.

[21] A. Morel, A. Badel, Y. Wanderoild, and G. Pillonnet, "A unified N-SECE strategy for highly coupled piezoelectric energy scavengers," *Smart Mater. Struct.*, vol. 27, Jul. 2018, Art. no. 084002, doi: 10.1088/1361-665X/aac3b6.

[22] D. Gibus, P. Gasnier, A. Morel, S. Boisseau, and A. Badel, "Nonlinearities influences on performances of a strongly-coupled piezoelectric generator for broadband vibration energy harvesting," in *Proc. 19th Int. Conf. Micro Nanotechnol. Power Gener. Energy Convers. Appl.*, 2019, pp. 1–5, doi: 10.1109/PowerMEMS49317.2019.61547410359.

[23] T. Ueno, "Magnetostrictive vibrational power generator for battery-free IoT application," *AIP Adv.*, vol. 9, Mar. 2019, Art. no. 035018, doi: 10.1063/1.5079882.

Takeaki Yajima (Member, IEEE) received the M.S. and Ph.D. degrees in oxide heterostructures and electronic devices from the Department of Advanced Materials Science, The University of Tokyo, Tokyo, Japan, in 2009 and 2012, respectively.

He was a Visiting Scientist with SLAC National Accelerator Laboratory, Stanford University, from 2011 to 2012 and an Assistant Professor with the Department of Materials Engineering, University of Tokyo, from 2012 to 2020. He is currently an Associate Professor with the Department of Electrical and Electronic Engineering, Kyushu University, Fukuoka, Japan, from 2020. His research interests include energy harvesting circuits, neuromorphic engineering, and oxide thin film devices.